Comparison of Boost-Based MPPT Topologies for Space Applications

OSCAR GARCÍA, Member, IEEE
PEDRO ALOU, Member, IEEE
JESÚS Á. OLIVER, Member, IEEE
DANIEL DÍAZ, Student Member, IEEE
DAVID MENESES, Student Member, IEEE
JOSÉ A. COBOS, Senior Member, IEEE
Universidad Politécnica de Madrid

ANDRES SOTO
EMILIO LAPEÑA
EADS Astrium CRISA
Spain

JESÚS RANCAÑO
European Space Research and Technology Centre (ESTEC)

Several boost-derived topologies are analyzed and compared for an aerospace application that uses a 100 V voltage bus. All these topologies have been designed and optimized considering the electrical requirements and the reduced number of space-qualified components. The comparison evaluates the power losses, mass, and dynamic response. Special attention has been paid to those topologies that may cancel the inherent right half plane zero (RHP) zero of the boost topology. Experimental results of the less common topologies are presented.

Authors' addresses: O. García, Universidad Politécnica Madrid, Centro Electrónica Industrial, José Gutierrez Abascal 2, ETSII-Electronica, Madrid, 28006, Spain, E-mail: (o.garcia@upm.es); P. Alou, J. A. Oliver, D. Díaz, D. Meneses, J. A. Cobos, Universidad Politécnica de Madrid, Madrid, Spain; A. Soto, E. Lapeña, EADS Astrium CRISA, Calle de Torres Quevedo, 28760 Tres Cantos, Madrid, Spain; J. Rancaño, Power & Energy Conversion Division, ESTEC, Noordwijk, The Netherlands.

I. INTRODUCTION

High power and high voltage (100 V) power buses are often required not only in the frame of telecommunication spacecrafts, but also for those scientific and interplanetary mission cases where a high user power load demand drives the design of the power subsystem [1, 2]. In many cases the use of maximum power point tracking (MPPT) is essential for optimum power subsystem sizing [3, 4].

The adaptation to 100 V of the existing MPPT concepts for 28 V buses (like GOCE, ROSETTA, etc.) is not immediate, as happens in general terms with the upgrading of power conditioning units from 28 V to 50 V and 100 V. Moreover, for those cases where the solar array voltage is under the bus voltage, a step-up boost power cell is mandatory for MPPT implementation.

One of the platforms that will use 100 V due to its high power is the BepiColombo mission that will be launched to study the planet Mercury. This is a very challenging mission of the European Space Agency (ESA) (in collaboration with the Japan Aerospace Exploration Agency (JAXA)), being that the proximity of the Sun is the key point that makes a big difference compared with other missions. The satellite will be equipped with large solar arrays and an MPPT converter to provide high power to the propulsion unit and to reach the planet Mercury in a reasonable time.

This paper focuses on the definition of the main performance characteristics that must have a converter power cell to work as an MPPT and to fit the above-mentioned application range. According to the preliminary design of the mission, the MPPT should be a boost type converter [5, 6]. Since isolation is not a requirement, only nonisolated circuits have been analyzed since the presence of the transformer will increase the mass and power losses and no special advantage will be obtained.

Starting with the establishment of the relevant trade-off parameters, in terms of power handling capability, input and output operational voltage range, conducted emissions, bus capacitor, and solar array output impedance considerations, several candidate topologies are analysed:

1) conventional boost converter,
2) interleaved boost converter in both discontinuous conduction mode (DCM) or continuous conduction mode (CCM),
3) two-inductor boost converter,
4) two-inductor boost converter with common damping,
5) boost converter with ripple cancellation,
6) boost converter with switch near ground.

These already-known topologies or variations are considered as candidates for the MPPT power converter for this mission. Only topology 4 is not state of the art; it has been derived from the two-inductor

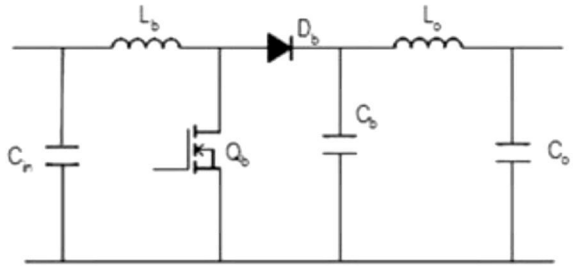

Fig. 1. Classical boost converter.

boost converter adding secondary windings to the inductors and connecting them with a damping resistor. All these topologies have been designed according to the electrical specifications. The best design of each one is accounted in terms of mass and efficiency by obtaining a quantitative comparison that helps to decide the best option.

Special attention is paid to the feasibility of the design for the control loop that will govern the converter operation when forming part of a power conversion unit (PCU), taking into account the effects of the right half plane zero (RHPZ) inherent to most of the boost converter topologies. The dynamic performance of the power stage of these six boost topologies is accounted to foresee the limitations that they will impose on the bandwidth of the loop. Some of the candidate topologies are prototyped to demonstrate in the laboratory the performances identified during the analysis phase.

As a summary the goal of this paper is to select the best boost topology for the MPPT converter of this specific application based on mass, dynamic performance, and efficiency.

II. POWER TOPOLOGIES REVIEW

Due to the characteristics of the solar arrays and the voltage of the bus of this PCU, the power topology should be based on a boost converter. The analysis has been carried out considering nonisolated topologies.

Six boost-derived power topologies are reviewed in this paper. In the following paragraphs these topologies are presented.

A. Classical Boost Converter

This well-known topology is shown in Fig. 1. Its simplicity is its main advantage, which implies a low number of components and a high reliability [7]. An additional advantage is the experience of use in aerospace projects. If it is designed in CCM, it may suffer high power losses due to the reverse recovery of the diode. Moreover, in CCM, the presence of the RHPZ may cause a limited bandwidth. DCM avoids these two problems, but it increases the rms currents across the power components.

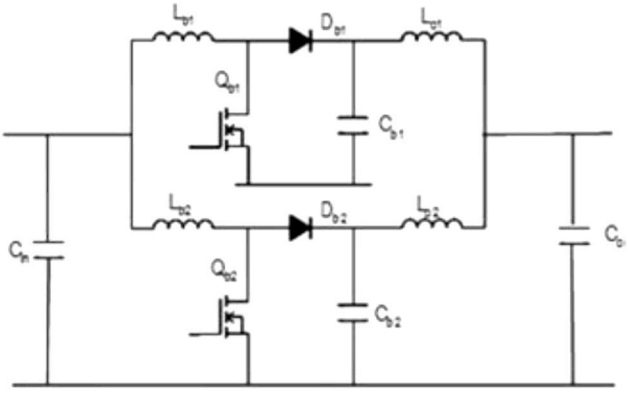

Fig. 2. Interleaved boost converter.

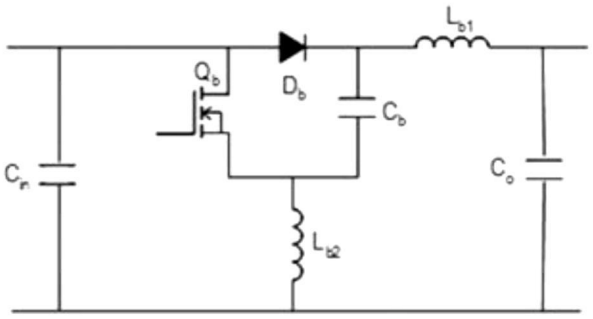

Fig. 3. Two-inductor boost converter.

Some of the analysed topologies have both continuous input and output current. Therefore, as it can be seen in Fig. 1, an LC output filter [8] is included to compare all the topologies in the same conditions.

B. Interleaved Boost Converter

Two half-power identical power stages can be paralleled to build the converter (see Fig. 2). By shifting the driving signal of the transistors 180°, the filters are drastically reduced [9, 10].

The comments about CCM and DCM and the output LC filter made for the classical boost converter are valid for this variation. However, in CCM, it is necessary to include the equalization of the currents (this is not a problem in current mode control, but it requires two current sensors).

C. Two-Inductor Boost Converter

The main advantage of this two-inductor boost converter (Fig. 3) is that both input and output currents are continuous [11]. However, there are two power inductors. The current ripple in each inductor is exactly the same as the classical boost since the voltage applied to them is V_{IN} during on time and $V_{IN} - V_O$ during off-time.

As well as the previous topologies, the inherent RHPZ of the boost topologies appears in this topology.

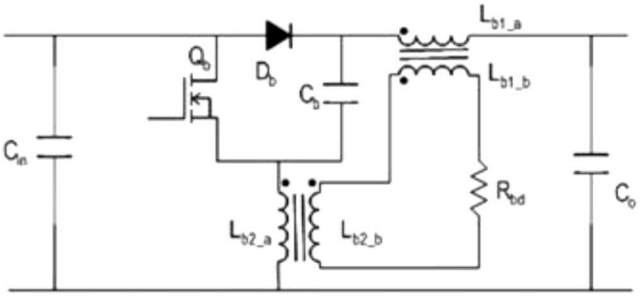

Fig. 4. Two-inductor boost converter with common damping.

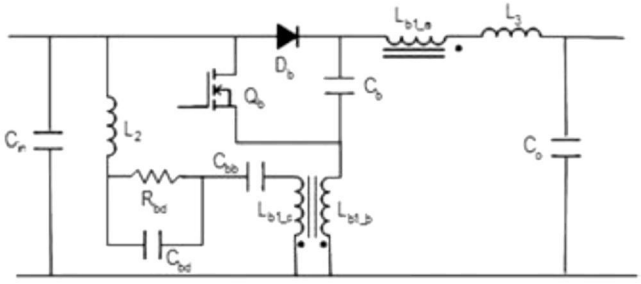

Fig. 5. Boost converter with ripple cancellation.

D. Two-inductor Boost Converter with Common Damping

Using topology 3 as a base and with the addition of two coupled inductors and a common damping resistor, we obtain a circuit (Fig. 4) that, in certain conditions, will be able to remove the RHPZ. The power stage remains more or less the same as the original circuit, and no big differences in the mass can be found. Regarding the inductors' core part of their window area is used to wind the secondary winding, which reduces the section of the wires and increases the conduction losses a bit, as is seen later. Therefore, the main advantage is that the bandwidth of the loop can be improved by means of a more complex power structure.

E. Boost Converter with Ripple Cancellation

This topology is derived from the two-inductor boost converter [12]. An additional branch has been included to cancel the input current ripple (see Fig. 5). Basically, the converter operates as a two-inductor boost converter with some additional components. The cancellation branch is composed of L2, Cbb, and a coupled winding $Lb1_c$. Cbb is a blocking capacitor that holds a voltage equal to the input voltage. The coupled inductor polarizes inductance L2 in such a way that the addition of its current ripple (it has no dc current) is the opposite of the current demanded by the converter. Thus, the addition of both is almost zero at every input voltage.

This current ripple cancellation branch allows a reduction in the overall mass of inductors and capacitors. The main drawback is the amount of components added to the topology.

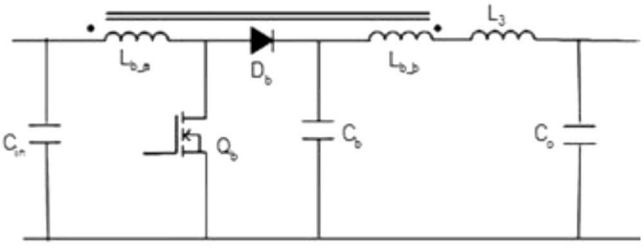

Fig. 6. Boost converter with switch near ground.

L3 filters the output current, and, therefore, most of the magnetizing current of inductor Lb flows through $Lb1_b$ winding.

F. Boost with Switch Near Ground

The last topology of this analysis is presented in [13] and shown in Fig. 6. Previous works [14] show this topology without LC filter and another approach to cancel RHPZ in the two-inductor boost. An additional coupled winding allows advantages, regarding the RHPZ of the boost converter. Moreover, compared with some of the previous topologies, the power transistor is grounded, which makes the implementation of the driving circuit easy. Additional design considerations for this topology are recently published in [15].

The main advantage of this circuit is that, thanks to the additional winding Lb_b, there is a direct energy transfer between input and output during transistor on-time. This allows, in certain conditions [16], the RHPZ of the boost converter to be removed. The turns ratio of the coupled inductor Lb plays an important role in the converter. With it the converter behaviour runs from a conventional boost to a low ripple boost.

In particular, in the next analysis, we try to determine the following features.

1) *Mass*: Taking into account the fact that there are 24 converters in the satellite, one of the priorities is to reduce the mass of the converter. The mass is determined mainly by the inductors (core and windings) and capacitors.

2) *Bandwidth*: In certain conditions high negative current steps are applied to the converter. Thus, a high bandwidth together with a small energy-storage converter is desirable. Bode plots are obtained to foresee the potential capabilities from the point of view of the control.

3) *Efficiency*: It should be as high as possible, but keep in mind that 97% is required. The power losses are evaluated in the inductors and MOSFET.

III. DESIGN FOR STATIC CONDITIONS

A. Specifications

Each power converter is designed for 500 W. Solar array provides a voltage between 40 V and 96 V, with the battery voltage being equal to 100 V in nominal conditions. Since all these boost circuits have the

TABLE I
Main Parameters of the Classical Boost Converter

CONVENTIONAL BOOST		Value	Mass	Losses
INDUCTORS	L_b	96µH	142,7gr	4,1W
	L_o	2,4µH		
CAPACITORS	C_b	4,7µF	65,1gr	
	C_o	47µF		
MOSFET				11,74W
Total mass			207,8gr	
Total losses				15,84W

same dc gain, there are no differences in the duty cycle range.

To compare the topologies the switching frequency has been fixed to 130 kHz. In order to make a proper comparison, all the designs should comply with the following conditions.

1) *Input current ripple*: is limited to 20% peak-to-peak of the nominal current in the worst case line condition.

2) *Output voltage ripple*: is limited to 0.5% of the nominal output voltage.

3) *Output capacitor*: the minimum output capacitance (for impedance reasons) has been fixed around 41 μF (normalized value of 47 μF). There are some topologies that may offer a smaller capacitor, but, in this case, this advantage is lost.

4) *Voltage ripple of floating capacitors*: in several topologies, there are one or two flying capacitors. They have been designed to obtain a 5% voltage ripple. In some cases the capacitor has been increased to meet the rms currents imposed by the circuit.

The parts used in the design of these circuits are the following.

1) *Inductors*: they should be designed using Magnetics MPP toroidal cores (its density is 8.7 gr/cm^3). The main criteria is size, but the inductor should match filling factor (25%), power losses (< 1%), and use AWG22 with 5 maximum parallel windings. It is noted if some of these requirements are not accomplished.

2) *Capacitors*: Self Healing PM94 Eurofarad capacitors have been used for this comparison.

3) *Transistors*: Power Fet N-channel IRHMS57260SE have been used for this comparison as all switches have the same voltage stress and similar rms current. The interleaved boost topology has a reduced rms current, but the other available MOSFETs within the used technology have more power losses.

In the following paragraphs the main data obtained from the design of these boost topologies are shown. The power losses shown in the tables correspond to

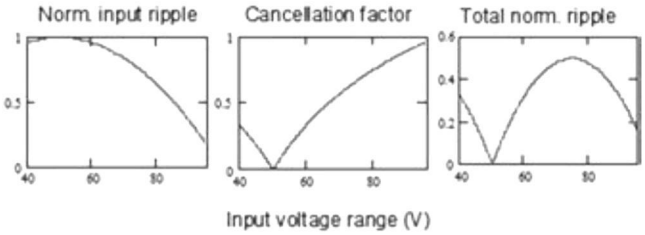

Fig. 7. Current ripple in interleaved boost converter.

40 V input voltage, which is the worst case because conduction losses are predominant. The inductors have been designed for the highest ripple condition that takes place at 50 V. The capacitors have been selected according to the capacitance and maximum rms current.

B. Classical Boost Converter

The main parameters of the CCM classical boost converter, regarding mass and losses, are introduced in Table I.

C. Interleaved DCM Boost Converter

Unfortunately, this design does not comply with the restriction of 20% input current ripple. Therefore, it is considered in CCM. However for smaller currents it seems a very good option. The main parameters of this design are shown in Table II.

D. Interleaved CCM Boost Converter

The inductances have been selected to meet the 20% input current ripple requirement. Current ripple depends on input voltage but also ripple cancellation factor. Therefore, to determine the worst case input current ripple, it is necessary to account for both. Figure 7 shows this issue. The worst case occurs at 75 V.

Thanks to the partial cancellation of the inductor currents, the inductance can be decreased compared with the other topologies (Table III).

E. Two-Inductor Boost Converter

In this case, to achieve 20% input current ripple, it is necessary to guarantee a 10% in each inductor. The

TABLE II
Main Parameters of the Interleaved DCM Boost Converter

INTERLEAVED DCM BOOST CONVERTER		Value	Mass	Losses
INDUCTORS	L_{b1}	12,4µH	94,94gr	17W
	L_{b2}	12,4µH		
	L_{o1}	1,2µH		
	L_{o2}	1,2µH		
CAPACITORS	C_{b1}	4,7µF	66,2gr	
	C_{b2}	4,7µF		
	C_o	47µF		
MOSFET				10,44W
Total mass			161,14gr	
Total losses				27,44W

TABLE III
Main Parameters of the Interleaved CCM Boost Converter

INTERLEAVED CCM BOOST CONVERTER		Value	Mass	Losses
INDUCTORS	L_{b1}	43µH	97gr	6,96W
	L_{b2}	43µH		
	L_{o1}	1,2µH		
	L_{o2}	1,2µH		
CAPACITORS	C_{b1}	3,3µF	64gr	
	C_{b2}	3,3µF		
	C_o	47µF		
MOSFET				12,96W
Total mass			161gr	
Total losses				19,92W

reason is that both inductors have exactly the same current ripple, and the addition of both flows through the input. Therefore, the mass is a very big penalty for this topology (Table IV).

One of the advantages of this converter is the small output current ripple that allows a smaller output capacitor. However, in this design, this advantage is lost because a minimum of 47 μF is placed in the output for impedance reasons.

F. Two-Inductor Boost Converter with Common Damping

The addition of the common damping network does not force an important increase in the mass of the converter since one of the parallel windings of the main inductors has been used for the secondary winding (Table V). However, the losses in the magnetic components are increased. The losses in the damping resistor are less than 0.5 W (0.1% of the nominal output power) for all the possible operating conditions.

As the damping network does not mean a significant change in the MOSFET current, its power losses are considered the same regardless of whether the converter has damping or not.

G. Boost Converter with Ripple Cancellation

From the point of view of the inductors, this converter shows a different design. It has three inductors, and one of them has three windings. However, since the main inductor current ripple is fully cancelled with the auxiliary branch, the inductance can be reduced, obtaining a small value. Then, due mainly to the design of the inductors, this converter has a smaller mass than the other candidate topologies.

The high damping resistor value (R_{bd} in Fig. 5) modifies the current ripple in the cancellation branch and, therefore, decreseases the efficiency of the input current ripple cancellation. Furthermore, it increases the losses in the converter (Table VI). A maximum value of 0.45 Ω has been chosen to comply with the efficiency requirements, which implies a maximum power dissipation of 0.6 W.

TABLE IV
Main Parameters of the Two-Inductor Boost Converter

TWO INDUCTOR BOOST		Value	Mass	Losses
INDUCTORS	L_{b1}	192µH	268,3gr	4,7W
	L_{b2}	192µH		
CAPACITORS	C_b	8,2µF	67,8gr	
	C_o	47µF		
MOSFET				11,74W
Total mass			336,1gr	
Total losses				16,44W

TABLE V
Main Parameters of the Two-Inductor Boost Converter with Common Damping

TWO INDUCTOR BOOST COMMON DAMPING		Value	Mass	Losses
INDUCTORS	L_{b1}	192µH	268,3gr	6,2W
	L_{b2}	192µH		
CAPACITORS	C_b	8,2µF	67,8gr	
	C_o	47µF		
MOSFET				11,74W
Total mass			336,1gr	
Total losses				17,94W

TABLE VI
Main Parameters of the Boost Converter with Ripple Cancellation

BOOST RIPPLE CANCELLATION		Value	Mass	Losses
INDUCTORS	L_{b1_a}	51µH	91,56gr	2,8W
	L_{b1_b}	51µH		
	L_{b1_c}	2,4µH		
	L_2	7,2µH		
	L_3	3µH		
CAPACITORS	C_{bb}	3,3µF	70gr	
	C_{bd}	3,3µF		
	C_b	4,7µF		
	C_o	47µF		
MOSFET				11,6W
Total mass			161,56gr	
Total losses				14,4W / 15W*

* Damping resistor losses included (Rbd=0.45Ω).

H. Boost with Switch Near Ground

Table VII shows the result of the design of this topology for this particular specification without the RHPZ cancellation. The degree of freedom (Lb turns ratio) is used to decrease the size of the inductors of the converter and not to cancel the RHPZ.

Even in this case this design shows a worse result from the point of view of the mass compared with the rest of the variations. Moreover, the cancellation of the RHPZ in this topology implies a high increase in the mass of the solution.

Table VIII shows the results for a design that cancels the RHPZs of this topology. It can be seen that the price to achieve a dynamic improvement is a high increase in the size and in the power losses of the inductors.

TABLE VII
Main Parameters of the Boost Converter with Switch Near Ground

BOOST SWITCH NEAR GROUND		Value	Mass	Losses
INDUCTORS	L_{b1_a}	128µH	223,94gr	5,2W
	L_{b1_b}	1,28µH		
	L_3	3,8µH		
CAPACITORS	C_b	6,8µF	63,7gr	
	C_o	47µF		
MOSFET				11,74W
Total mass			287,64gr	
Total losses				16,94W

TABLE VIII
Main Parameters of the Boost Converter with Switch Near Ground with Improved Dynamic Behaviour

BOOST SWITCH NEAR GROUND		Value	Mass	Losses
INDUCTORS	L_{b1_a}	220µH	690gr	33W
	L_{b1_b}	1,6mH		
	L_3	1,2mH		
CAPACITORS	C_b	6,8µF	63,7gr	
	C_o	47µF		
MOSFET				11,74W
Total mass			753,7gr	
Total losses				44,74W

IV. DYNAMIC CHARACTERIZATION AND BANDWIDTH DISCUSSION

The existence of RHPZ, inherent to the boost converter in CCM [17], is well known. This nonminimum phase behaviour is expected in all the analysed topologies since they are all boost-derived topologies. However, topologies 4 and 6 can cancel the RHPZ in certain conditions as mentioned before. On the other side designs complying with these conditions mean a higher mass of the converter, which cannot be afforded for this application.

The objective of this section is to evaluate the bandwidth capabilities of each topology for designs complying with the specifications presented in the previous section. To achieve this each topology is analysed and modelled. Using the derived averaged models, bode plots of the control to output voltage transfer function are obtained from the simulator. The presented plots correspond to an input voltage of 40 V and are plotted from 10 Hz to 1 MHz.

A. Classical Boost Converter

The obtained bode plot (Fig. 8) shows a dynamic response with two poles and an RHPZ, a typical boost frequency response. The RHPZ frequency (around 3 kHz), together with the resonance frequency (900 Hz), reduces the bandwidth to 300 Hz in order to achieve a safe design for closed-loop operation. At very high frequency the effect of the output filter can be seen.

B. Interleaved CCM Boost Converter

The dynamic response of the CCM interleaved boost converter (Fig. 9) shows a similar response to the boost converter with output LC filter. However, both the RHPZ and the resonance frequency take place at higher frequency, which allows a lighter increase in the bandwidth.

C. Two-Inductor Boost Converter

The dynamic response of this converter is more complex than in the previous converters, which shows two RHPZs and four poles (Fig. 10). However, the resonance frequency is the same as in the classical boost, and the expected bandwidth is close to the one achieved in that case, despite the second resonant frequency. This is one of the limitations of this topology.

D. Two-Inductor Boost with Common Damping

Besides the fact that the two-inductor boost converter is mass penalized with respect to the classical boost converter, the expected bandwidth in closed-loop operation is close in both cases. However, the addition of a common damping network allows a higher bandwidth by cancelling the RHPZs.

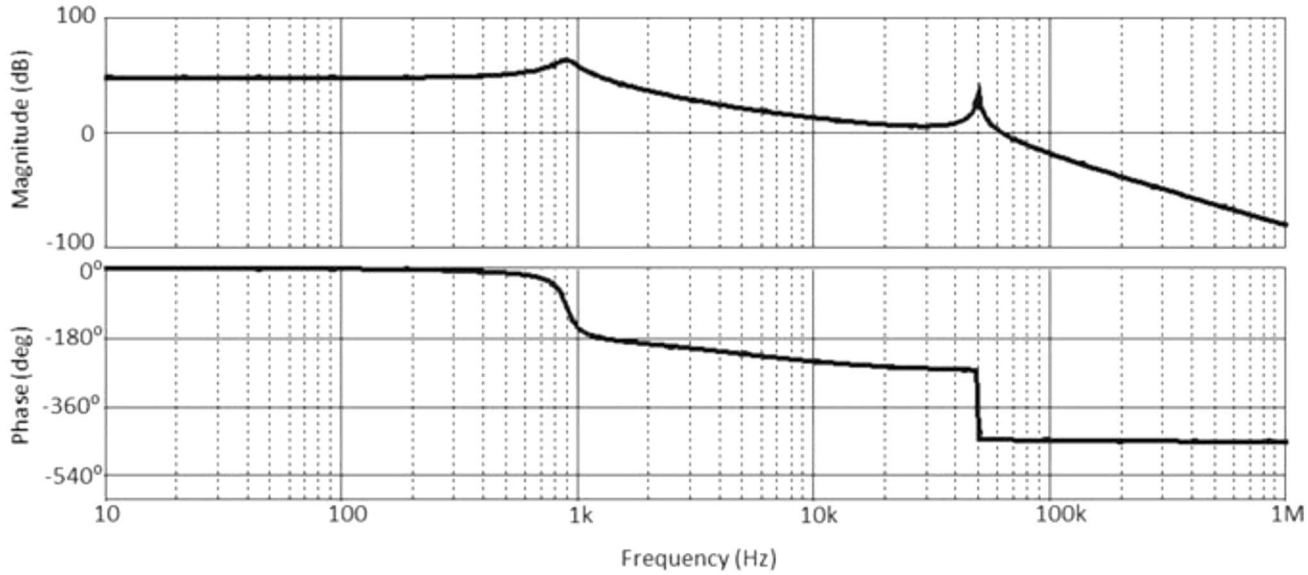

Fig. 8. Control to output voltage bode plot of conventional boost converter.

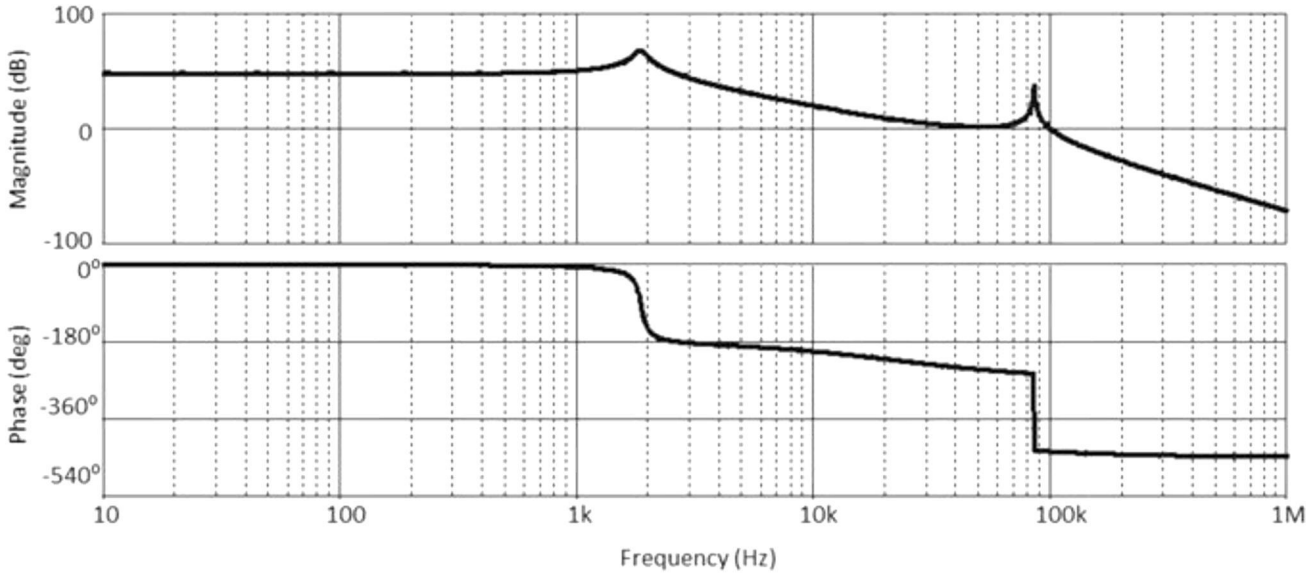

Fig. 9. Control to output voltage bode plot of interleaved CCM boost converter.

Based on the obtained averaged model, the theoretical control to output voltage transfer function has been achieved. A detailed analysis of the numerator shows that the RHPZs cancellation depends on the damping resistor value. Equation (1) shows the obtained condition for the damping resistor, in a specific design, to achieve a minimum phase behaviour.

$$\frac{L_{b1}}{R_L \cdot C_b} \cdot \frac{1}{1-d} < R_{bd} < \frac{(1-d)^2}{d} \cdot \frac{R_L}{L_{b2}} \cdot (L_{b1} + L_{b2}). \quad (1)$$

Figure 11 shows the Bode diagram of the two-inductor boost with common damping for the current design, with a damping resistor value that complies with (1). As can be seen, now the phase ends at 180 deg instead at 540 deg. Therefore, a bandwidth up to 30 kHz (one-fifth of the switching frequency) can be achieved. Furthermore, the bandwidth improvement of more than two decades in relation to the converter without common damping does not imply any change in the mass or a significant increase in the losses with respect to that converter.

E. Boost Converter with Ripple Cancellation

In low and medium frequencies, the control to output voltage transfer function shows a classical boost equivalent transfer function (Fig. 12). However, at higher frequency, there are additional poles and zeroes. These poles and zeroes do not have influence on the control stage design, and the expected bandwidth will be similar to that obtained in a classical boost converter. Damping resistor Rbd

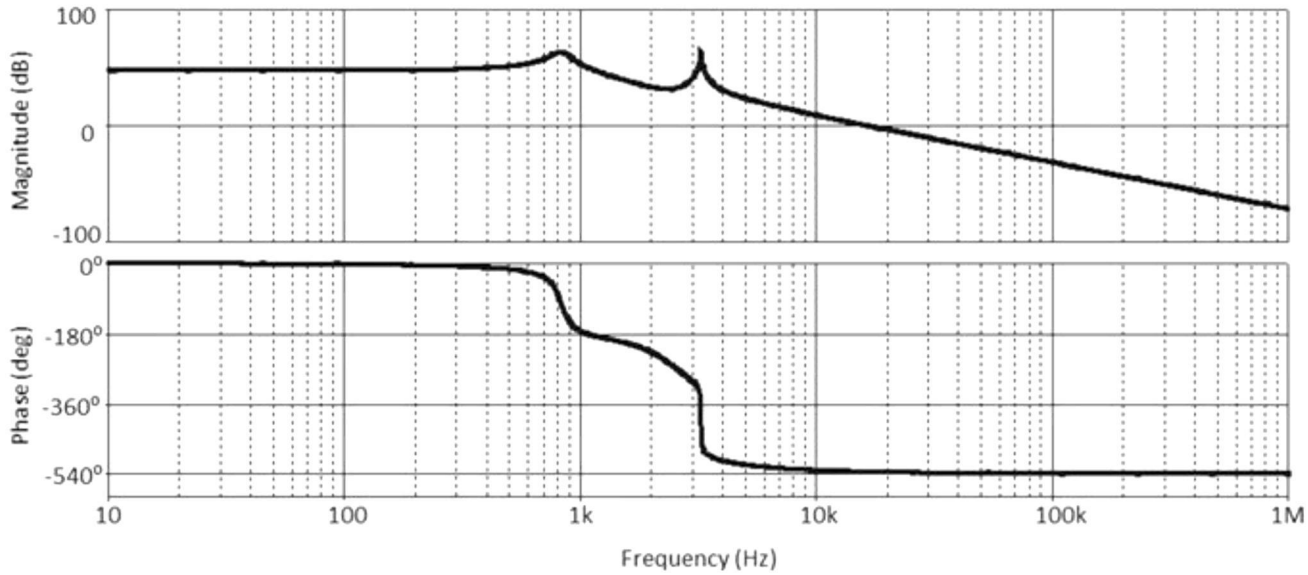

Fig. 10. Control to output voltage bode plot of two-inductor boost converter.

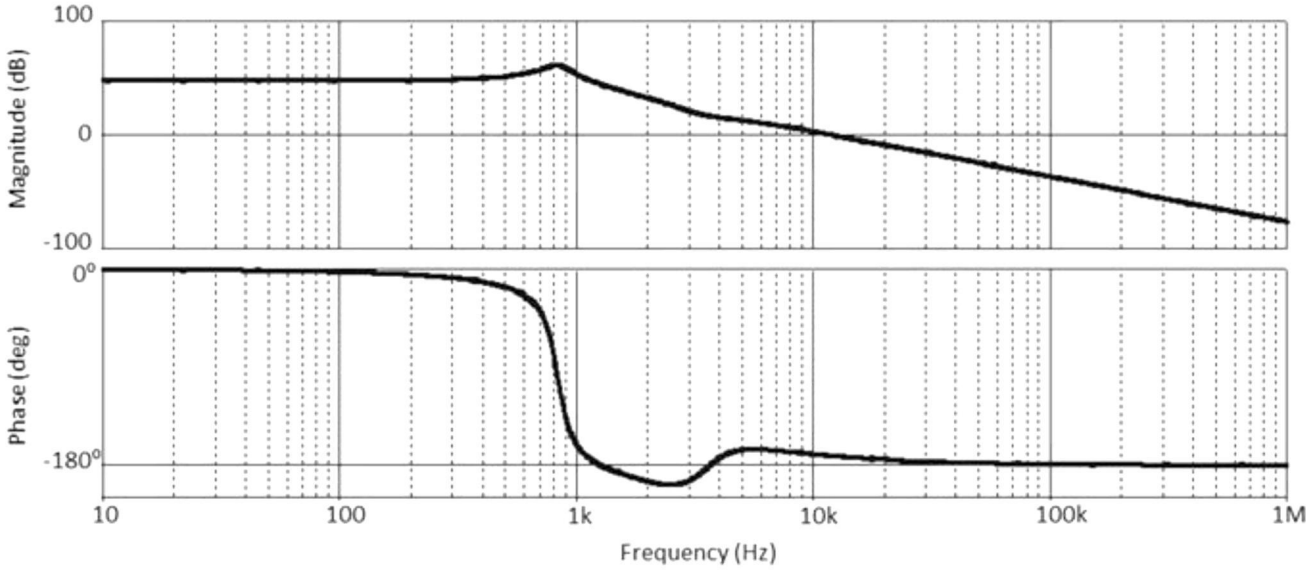

Fig. 11. Control to output voltage bode plot of two-inductor boost converter with common damping, without RHPZs.

has no influence on the control stage design, and, therefore, its value has been selected to comply with the efficiency requirements as explained in the previous section.

In order to increase the bandwidth of this topology, the dynamic behavior has been studied in detail. In [18] the seventh-order state-space model is calculated, and the second-order equivalent model is derived, equivalent to a conventional boost converter. By this procedure, based on the fast and slow variables method, it is demonstrated that the low frequency RHPZ cannot be cancelled.

F. Boost with Switch Near Ground

The Bode diagram (Fig. 13) shows two RHPZs and four poles. As can be seen, the transfer function is more complex at very high frequencies, but in general, the bandwidth will be similar to the classical boost converter.

For this particular design, shown in Fig. 13, the RHPZs are not cancelled. In [16] the design condition is presented for the cancellation of the RHPZs in this topology,

$$rt < 1 - d \tag{2}$$

where "rt" is the turn ratio of the coupled inductor "Lb" and "d" is the duty cycle. If condition (2) is fulfilled, a system with minimum phase is obtained, as can be seen in Fig. 14. Despite the increase in the bandwidth, as shown in the previous section, a design that fulfills (2) has the drawback of a bigger transformer and output inductor that implies an increase in the mass, which is critical for aerospace applications.

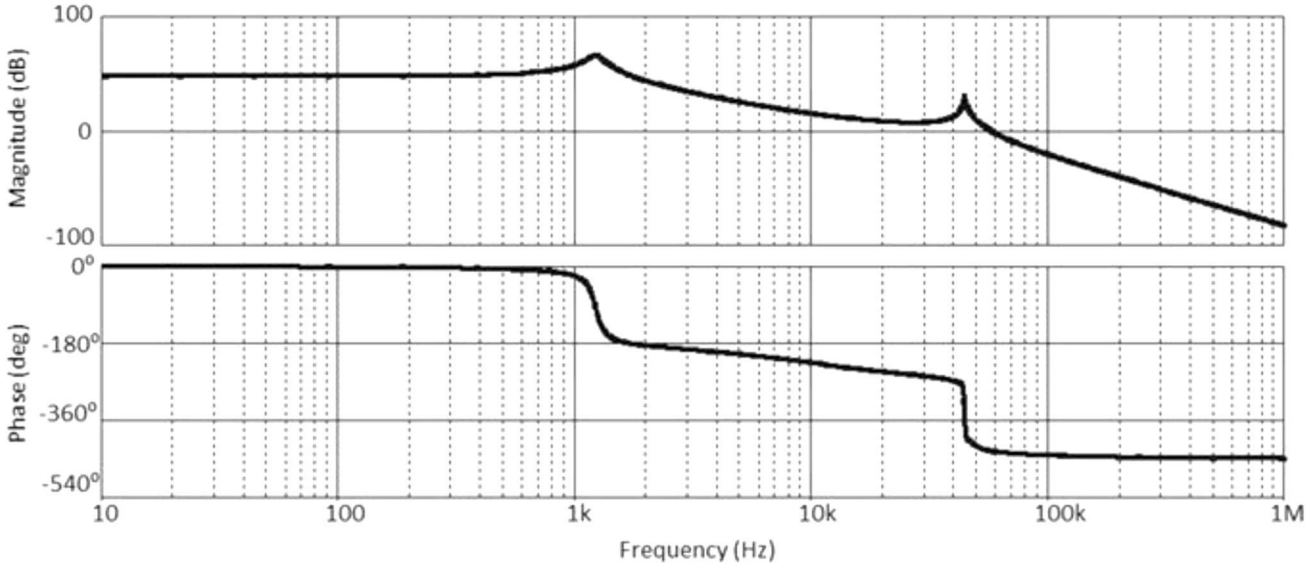

Fig. 12. Control to output voltage bode plot of the boost converter with ripple cancellation.

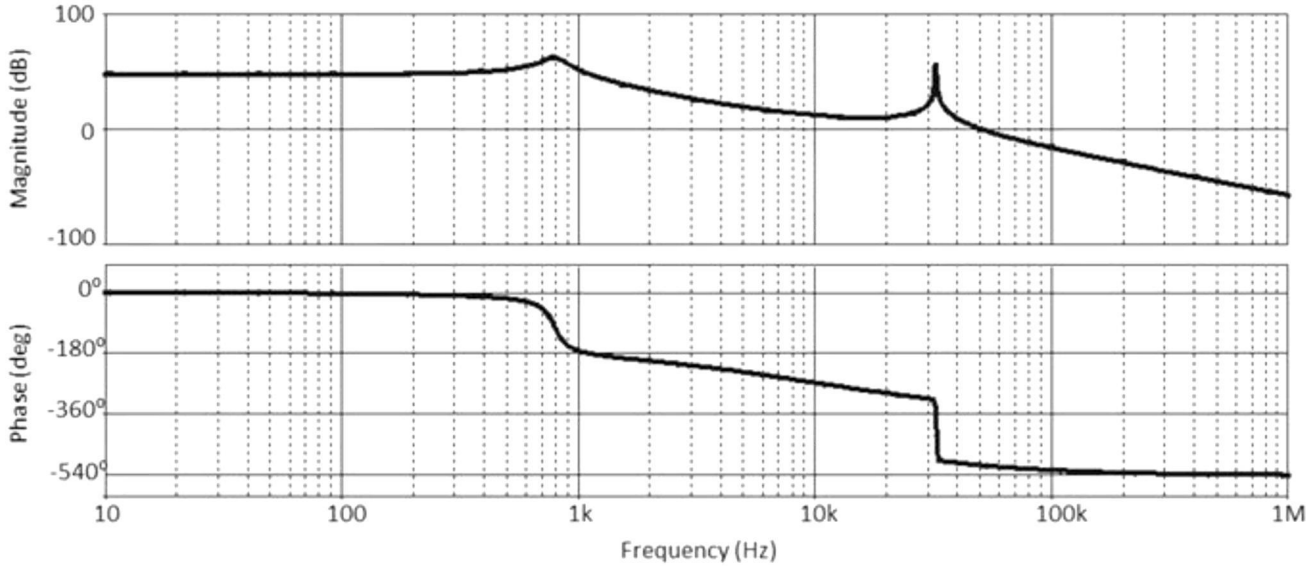

Fig. 13. Control to output voltage bode plot of the boost converter with switch near ground with RHPZs.

As a general design criteria, if the minimum input voltage is much smaller than the output voltage (high maximum duty cycle), the design of the magnetic components will be highly penalized in losses and weight, as shown in Table VIII. However, a very nice bandwidth (up to 30 kHz) can be obtained if (2) is fulfilled. More details about the design to cancel RHPZs can be found in [16].

G. Summary

As seen in this section, the last four topologies exhibit a much more complex transfer function than the conventional boost converter. However, the two-inductor boost with common damping and boost with switch near ground can cancel the RHPZ and increase the bandwidth. In the first case the mass, despite not being increased to achieve RHPZ cancellation, is high compared with other alternatives. In the second case the RHPZ cancellation would imply a high increase in the mass of the converter. The boost converter with ripple cancellation, as explained before, does not cancel the RHPZ in any condition, but it has additional advantages regarding current ripple and mass. As regards the conventional boost (interleaved or not), it has a small advantage from the point of view of mass and simplicity.

In the comparison section the bandwidth for a safe design, based on the Bode plots obtained in this analysis, is shown.

V. EXPERIMENTAL RESULTS

Some of these circuits have been prototyped. In particular the four less conventional boost converters have been built and tested. In this section some

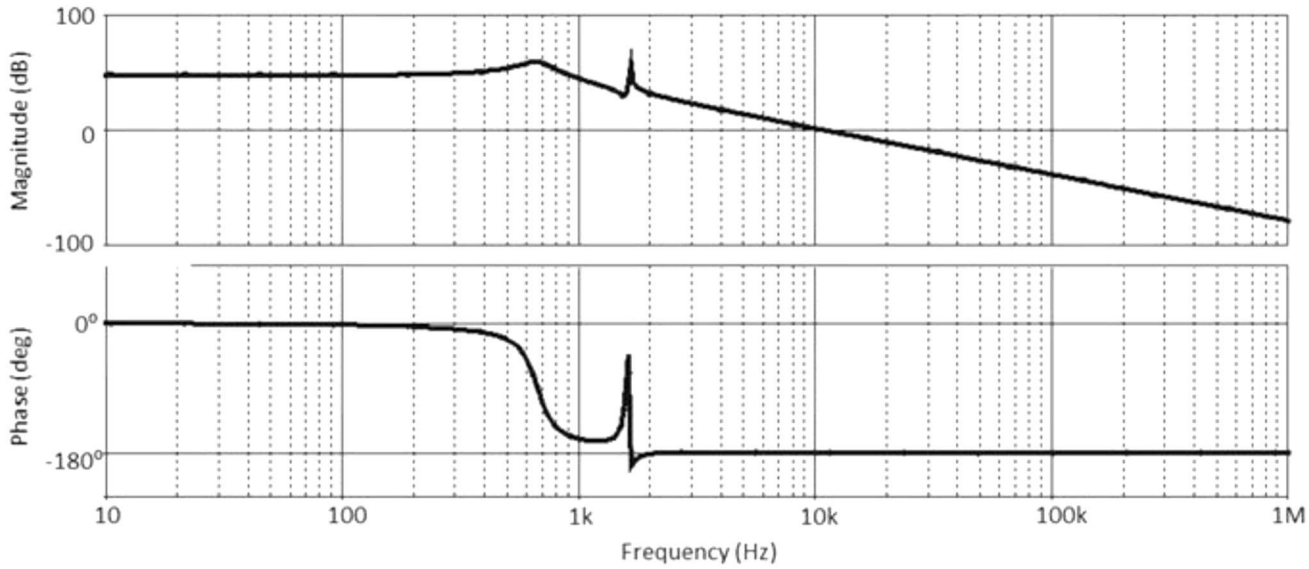

Fig. 14. Control to output voltage Bode plot of boost converter with switch near ground without RHPZs.

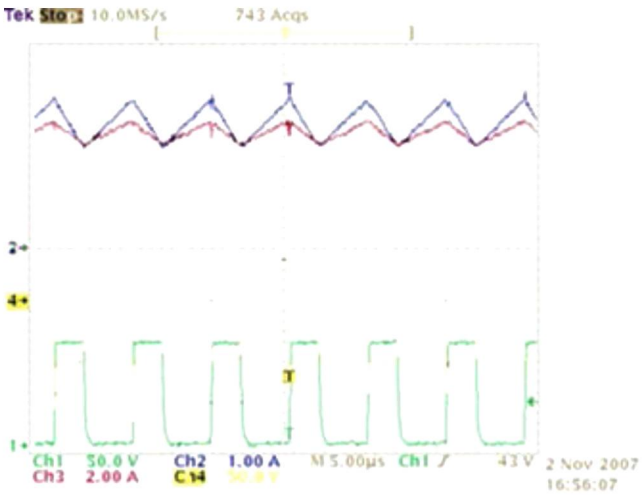

Fig. 15. Main waveforms of two-inductor boost converter: current through two-inductors (1 A/div and 2 A/div) and drain to source voltage (50 V/div) at 5 μs/div.

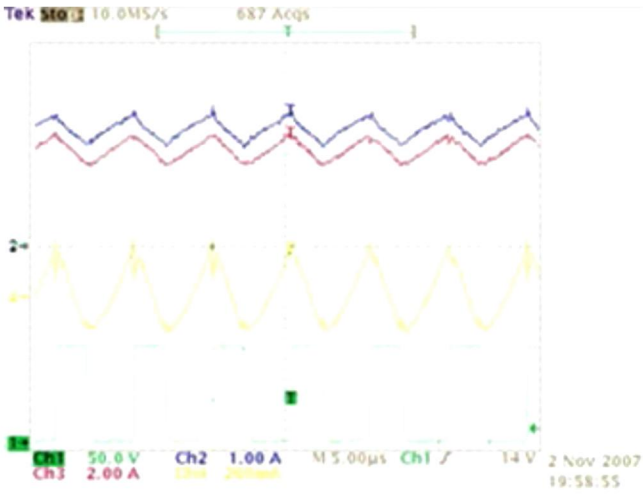

Fig. 16. Main waveforms of two-inductor boost converter with common damping: current through two-inductors (1 A/div and 2 A/div) and damping network current (200 mA/div) at 5 μs/div.

experimental waveforms obtained from the prototypes are included.

A. Two-Inductor Boost Converter

Figure 15 shows the main waveforms of the prototype. As it can be seen both, inductors' currents have exactly the same current ripple (note the different vertical scale).

B. Two-Inductor Boost with Common Damping

Figure 16 shows the same waveforms plus the damping network current for the converter with common damping.

C. Boost Converter with Ripple Cancellation

In Fig. 17 the main waveforms of this converter can be seen. It can be seen that the main boost current is cancelled with the cancellation branch.

Figure 18 shows the same waveforms in other conditions, being the converter in DCM. It can be seen that the cancellation characteristic are preserved even when the conduction mode changes.

D. Boost with Switch Near Ground

Figure 19 shows the main waveforms of this converter. This particular prototype is designed to operate in different conditions to check the RHPZ cancellation reported in [16].

Figure 20 shows the experimental validation of the cancellation of the RHPZs for this topology. In the figure on the left, the output voltage response to a step-up in the duty cycle can be seen. It can be observed that, due to the correct design, explained previously, no RHPZs effect appears. On the right side of Fig. 20, the same test for a different coupled

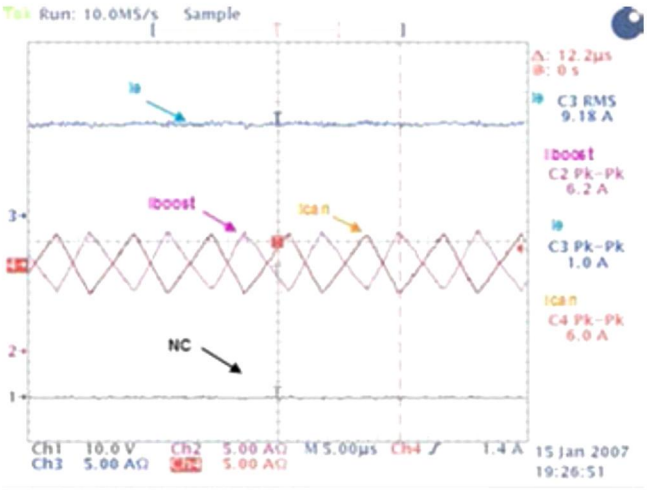

Fig. 17. Main waveforms of boost converter with ripple cancellation: Input current (5 A/div), boost main current (5 A/div), and ripple cancellation branch current (5 A/div) at 5 μs/div.

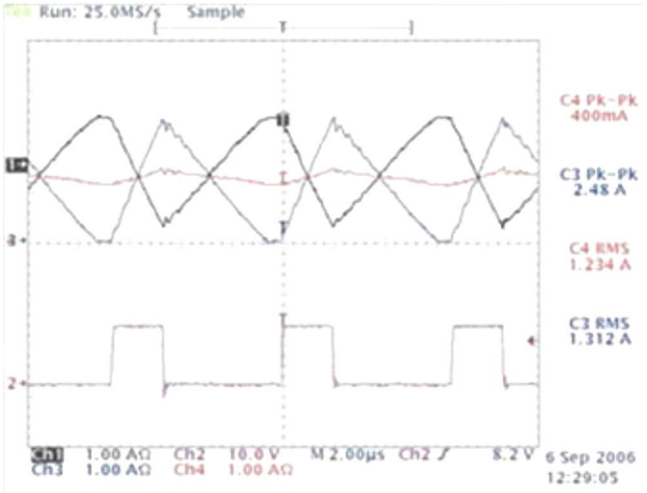

Fig. 18. Main waveforms of boost converter with ripple cancellation: Input current (1 A/div), boost main current (1 A/div), ripple cancellation branch current (1 A/div), and gate to source voltage (10 V/div) at 2 μs/div.

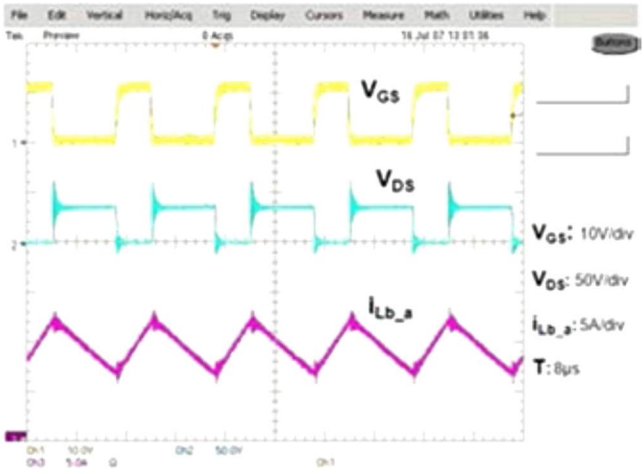

Fig. 19. Main waveforms of boost converter with switch near ground: gate to source voltage (10 V/div), drain to source voltage (50 V/div), and input current (5 A/div) at 8 μs/div.

inductor design which does not comply with the conditions to cancel the RHPZs (2) is shown, and therefore, the two RHPZs effect can be clearly seen.

VI. SUMMARY AND COMPARISON

To select the best topology for the current specifications, all the parameters and the importance of each one have to be taken into account as there is not a topology that offers the best performance in all the comparison fields. From the point of view of mass, topologies 2 and 5 are the best; looking at the efficiency, topologies 1 and 5 are better; finally, to obtain a good bandwidth, it is better to select topologies 4 and 6 with improved dynamic behaviour, however, these solutions are penalized in terms of mass and efficiency for this particular application.

Starting with the classical boost topology, it seems that, on average, it offers a good compromise among

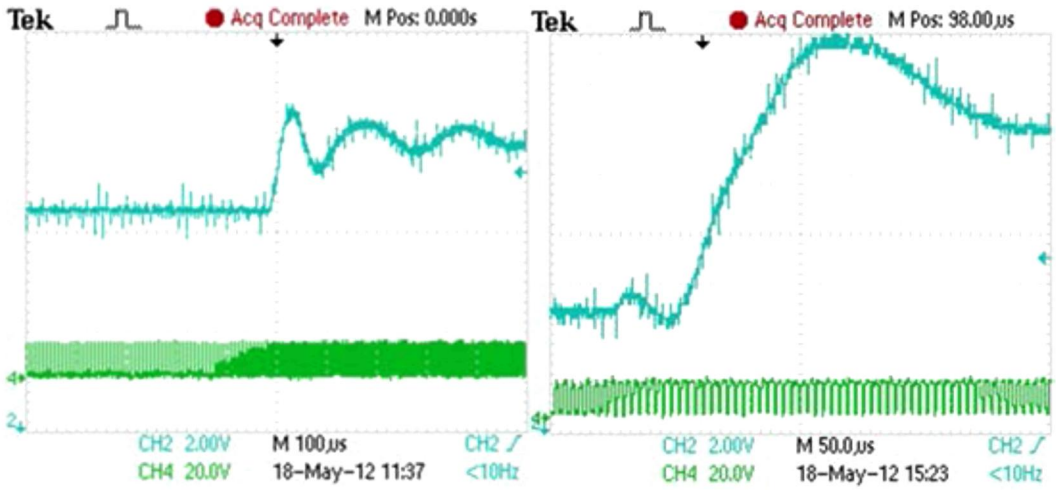

Fig. 20. Experimental validation of the RHPZ cancellation in the two-inductor boost with switch near ground: left figure: no RHPZs effect; right figure: RHPZs effect; top waveform: output voltage step-up (2 V/div) and bottom waveform: duty cycle (20 V/div) at 100 μs/div (left) and 50 μs/div (right).

TABLE IX
Comparison of the Six Analyzed Boost Topologies

	Topology	Number of transistors	Number of inductors	Number of caps.	Max. Input current ripple (%) @ Vin	Mass (gr)	Power losses (W)	Expected Bandwidth (Hz)
#1	Classical boost converter	1	2	2	20% @ 50V	207.8	15.8	300
#2	Interleaved boost converter	2	4	3	20% @ 50V	161.3	19.9	600
#3	Two inductor boost	1	2	2	20% @ 50V	336.1	16.4	300
#4	Two inductor with damping	1	2	2	20% @ 50V	336.1	17.9	30000
#5	LRB ripple cancellation	1	3	4	≈0 @ 40V-96V	161.6	14.4	400
#6	Boost switch near ground	1	2	2	20% @ 50V	287.1	16.9	300
#6	BSNG with RHP zero cancellation	1	2	2	20% @ 50V	753.7	44.74	30000

these analyzed parameters. Moreover, only a few components are required, so its reliability should be very high. The other topologies can be used to improve a particular feature, such as mass, efficiency, or dynamic performance.

Considering the data obtained in this analysis, topology 5 is a very good option. Low ripple boost with ripple cancellation allows a big reduction of the size and mass of the inductors. Also, power losses are among the smallest, and the bandwidth can be higher than other options. It is a nice alternative, but it has other drawbacks, such as a floating transistor, a higher number of components (less reliable), and a complex inductor with three windings.

The interleaved boost is the best option in terms of mass and bandwidth, but the power losses in its inductors penalizes the efficiency.

Table IX summarises the previous analysis in terms of number of devices, mass, power losses, and control.

The two-inductor boost topology has the advantage of a reduced output capacitor that, in this case, is fixed by the system. The addition of the common damping network allows an improvement in the bandwidth by means of the RHPZ cancellation. However, both topologies are clearly penalized if a small input current ripple is required, which forces them to have large inductors.

Boost with switch near ground allows the cancellation of the RHPZ but for this particular specification, it highly penalizes the mass and the losses of the magnetic components.

The maximum input current ripple for topology 2 is 20%. However, it allows a smaller inductor design due to the interleaved operation. Topologies 3 and 4 need to limit the current ripple to 10% on each inductor as the input current is the addition of them, which penalizes the inductor design. The boost converter with ripple cancellation network, 5, has zero input current ripple in theory, which is negligible, as shown in the experimental results section.

VII. CONCLUSIONS

In this paper six boost topologies have been analyzed and compared from the point of view of power losses, mass, and control loop bandwidth. All these topologies have been designed, modelled, and simulated, and/or built to test performance.

The classical boost converter appears to be a very good option. It offers a good trade-off between simplicity efficiency and losses. Its bandwidth is limited by the RHPZ. Therefore, it is selected in most of the cases.

The rest of the topologies are good from particular points of view, but none of them is better for this aerospace application.

In this paper the Bode plots of these not-very-usual boost topologies are shown. The complex dynamic behaviour of these topologies, considering RHPZ cancellation, is analyzed to improve the bandwidth of the converter.

REFERENCES

[1] Belloni, F., Maranesi, P. G., and Riva, M.
DC/DC converter for the International Space Station.
IEEE Transactions on Aerospace and Electronic Systems, **46**, 2 (2010), 623–634.

[2] Blanes, J. M., et al.
Two-stage MPPT power regulator for satellite electrical propulsion system.
IEEE Transactions on Aerospace and Electronic Systems, **47**, 3 (2011), 1617–1630.